Earthq Eng & Eng Vib (2021) 20: 193-211 **DOI**: https://doi.org/10.1007/s11803-021-2014-y

Residual drift spectra for RC bridge columns subjected to near-fault earthquakes

S.M. Seyed Ardakani[1†], M. Saiid Saiidi[2‡] and Paul Somerville[3§]

1. *Department of Civil and Environmental Engineering, Ohio Northern University, 525 S. Main St., Ada, OH 45810, USA*
2. *Department of Civil and Environmental Engineering, University of Nevada, Reno, MS 258, Reno, NV 89557, USA*
3. *AECOM Technology Corporation, One California Plaza, 300 S Grand Avenue, Los Angeles, CA 90017, USA*

Abstract: Permanent displacement of a bridge column can be directly measured during the inspection after near-fault earthquakes. However, the engineer needs to estimate the expected residual drift at the design stage to determine if the bridge seismic performance is satisfactory. The most direct method to estimate the residual displacement is nonlinear response history analysis, which is time consuming and cumbersome. Alternatively, an attractive but indirect method is generating estimated residual displacement spectra that depend on displacement ductility demand, column period, site conditions, and earthquake characteristics. Given the period and the expected displacement ductility demand for the column, the residual drift response spectra curves can be utilized to estimate the residual drift demand. Residual drift spectra that are applicable to RC bridge columns in different parts of the United States were developed based on nonlinear response history analyses using a comprehensive collection of recorded and synthetic near-fault ground motions and were linked to one-second spectral acceleration (S_1) of the AASHTO maps. It was also found that the residual drift ratio is below one percent when S_1 is less than 0.6 g.

Keywords: near-fault earthquake; reinforced concrete bridge column; residual displacement

1 Introduction

Significant residual displacements could occur in bridge columns due to the strong and long period velocity pulse in the fault-normal component of near-fault ground motions (Somerville *et al*., 1997; Somerville, 2002). The most unique response in shake table testing of six large-scale reinforced concrete bridge columns by Phan *et al*. (2007) and Choi *et al*. (2010) was the relatively large residual displacements even under moderate motions. Residual displacement could pose problems with respect to both aesthetics and safety. While a limit state for the former would be subjective, safety aspects can be quantified and accounted for in design to address the post-earthquake serviceability of the bridge. The feasibility of estimating residual displacements in bridge columns with reasonable accuracy plays an important key to determine if the bridge meets an acceptable level of performance and if it should be kept open to traffic or closed for repair or replacement subsequent to earthquakes. Following the 1995 Kobe earthquake, Kawashima *et al*. (1998) reported that approximately 100 reinforced concrete bridges with a residual drift ratio larger than 1.75% were demolished because they were believed to be unsafe even when the apparent bridge damage was not severe. A residual displacement response spectrum was proposed for the design of new bridge piers in Japan. The spectrum related the residual displacement ratio and the column stiffness ratio, which is the post-yield stiffness divided by initial elastic stiffness. Mackie and Stojadinovic (2004) reported that the residual displacement is a better parameter to measure the loss of load-carrying capacity of bridges than the earthquake intensity. They investigated four methods and found that the one that utilizes the maximum and residual displacement models provides the best estimate of the capacity loss. Wang *et al*. (2019) reported that the residual drift ratio is the optimal engineering demand parameter (EDP) for the assessment of load-carrying capacity of bridge columns. Probabilistic relationships between residual and maximum drift ratios were established to estimate the maximum drift ratio based on the measurable residual drift ratio following earthquakes. The estimated maximum drift ratio can be used to evaluate the damage to underground piles in typical extended pile-shaft-supported bridges in laterally

Correspondence to: S.M. Seyed Ardakani, Department of Civil and Environmental Engineering, Ohio Northern University, 525 S. Main St., Ada, OH 45810, USA
Tel: +1-(419) 772-2374; Fax: +1-(419) 772-2404
E-mail: s-seyedardakani@onu.edu
[†]Assistant Professor; [‡]Professor; [§]Principal Seismologist

Supported by: Federal Highway Administration (FHWA) under Contract No. DTFH61-07-C-00031
Received December 26, 2019; **Accepted** August 18, 2020

spreading grounds. Seyed Ardakani and Saiidi (2018) developed a simple empirical approach to estimate the residual displacement in RC bridge columns following near-fault earthquakes. The proposed method related the residual displacement to the displacement ductility demand and the yield displacement of the column, but did not take into account the effects of the column period, site conditions, and earthquake characteristics. Ruiz-Garcia and Miranda (2005) and Liossatou and Fardis (2015) performed response history analyses of single-degree-of-freedom systems and found that residual drift ratios exhibit a large level of dispersion from one record to another. Harikrishnan and Gupta (2020) estimated residual displacements for elastic-perfectly-plastic single-degree-of-freedom oscillators with a constant lateral strength ratio. They suggested that any estimation of residual displacement should be conducted in the statistical sense preferably via normalization with respect to inelastic spectral displacements. Recent nonlinear response history investigations by Phan *et al*. (2007), Lee and Billington (2010), Yazgan and Dazio (2011), Saiidi and Seyed Ardakani (2012), and Cheng *et al*. (2016) have shown that even though generally good estimation of residual displacements are obtained, the results can be very sensitive to modeling assumptions. The uncertainty in estimation of residual displacement should be addressed by finding residual drift spectra for a large number of earthquakes and taking a conservative approach. The spectra provide the user with a relatively simple method to determine the residual displacement following a near-fault earthquake. The objective of the present study was to generate residual drift spectra for different displacement ductilities, site conditions, and earthquake characteristics that represent the seismicity of different parts of the United States. To accomplish this goal, nonlinear response history analyses were conducted utilizing suites of recorded and synthetic near-fault acceleration histories.

2 Synthetic near-fault ground motions

Rupture directivity and hanging wall effects are two main characteristics of near-fault earthquakes. The rupture directivity effect occurs when the rupture aligns with the site and propagates towards the site, which may generate an intermediate to long period and large amplitude pulse (0.5 to 10 s) (Somerville, 1998). Since transverse shear waves accumulate in the direction perpendicular to the fault, the fault-normal component of near-fault ground motions is larger than the fault-parallel component (Somerville *et al*., 1997). The hanging wall effect is manifested in amplified short period ground motions (less than 1.0 s) on the hanging wall of a dipping fault (Abrahamson and Somerville, 1996).

These near-fault effects pertain mainly to shallow crustal earthquakes, which occur throughout the United States. The ground motion characteristics of shallow crustal earthquakes in the tectonically stable regions of the United States (east of the Rocky Mountains) are very poorly known due to the lack of strong motion recordings, but they are believed to be different from those of the tectonically active region west of the Rocky Mountains.

Although similar rupture directivity and hanging wall effects are generated by subduction earthquakes (occurring on the plate interface) and by earthquakes occurring within subducted slabs, these two kinds of earthquakes occur at greater depths and hence their directivity effects are diminished and were not treated in this study as near-fault effects. In the United States, subduction zone earthquakes affect the Pacific Northwest and Puerto Rico.

3 Approximate zonation of united states

Nine sites across the United States were chosen with different earthquake source characteristics. The selection of the nine sites was based on an approximate zonation of the seismic hazard in the United States. Figure 1 shows the location of these sites.

Near-fault earthquakes refer to ground motions occurring within approximately 15 km (9 miles) of the earthquake source (Caltrans, 2013). In addition to distance, magnitude also has a strong influence on near-fault earthquake effects. The approximate zonation of the United States was developed based on predominant earthquake magnitude as a first order method of evaluating representative near-fault response spectra and ground motion histories throughout the country. A brief description of the approximate zonation of the United States for generating synthetic near-fault ground motions is presented in the following stions. This formed the basis for selecting the nine sites for which acceleration histories were provided. For each of the nine sites, the predominant magnitude, style of faulting (strike-slip, reverse, or normal), and the name of the predominant fault are described.

The ground motions were presented on rock sites (class B/C boundary; V_{s30} = 760 m/s (2500 ft/s)), and soil sites (class C/D boundary; V_{s30} = 360 m/s (1200 ft/s)) for a return period of 975 years. For each record, there are two pairs of orthogonal spectrally matched horizontal acceleration histories. One pair is rotated 45 degrees from the fault normal (FN) and fault parallel (FP) directions, which are H1 and H2. These acceleration histories contain hanging wall effects for reverse faulting earthquakes, and average rupture directivity effects. The other pair is in the fault normal (FN) and fault parallel (FP) directions. These acceleration histories contain hanging wall effects for reverse faulting earthquakes and the fault normal (FN) component contains the rupture directivity pulse. Details of acceleration histories and their characteristics are presented in Seyed Ardakani and Saiidi (2013).

Fig. 1 Map of the nine sites across the United States

3.1 Pacific northwest

The Pacific Northwest includes the Pacific Coast of Alaska and the coastal regions of Washington, Oregon and Northern California (north of Cape Mendocino). In this region, crustal earthquake activity is influenced by subduction zones. In most of this region, near-fault ground motions are dominated by earthquakes with magnitudes of up to 7.0 (for example in Seattle and Portland). In some other regions, such as Humboldt Bay and the southern coast of Alaska, these earthquakes can have magnitudes as large as 8 on imbricate faults that are related to the underlying subduction zone.

3.1.1 Site 1. Seattle

This site is representative of sites mapped near reverse and reverse oblique faults in Seattle and Portland, which generate earthquakes of up to magnitude 7. For each site condition, seven records were derived from recordings of the M_w 6.9 1989 Loma Prieta, California and M_w 6.7 1994 Northridge, California earthquakes.

3.1.2 Site 2. Eureka, California

This site is representative of sites mapped near large thrust faults in northwestern California, which generate earthquakes of up to magnitude 8. Total of 14 records were derived from recordings of the M_w 7.6 1999 Chi-Chi, Taiwan and M_w 7.0 1992 Cape Mendocino, California earthquakes.

3.2 Central and southern california

The coastal regions of central and southern California (south of Cape Mendocino) are dominated by the strike-slip San Andreas Fault system. Reverse faulting is also prevalent in the transverse ranges, including Santa Barbara and Los Angeles.

3.2.1 Site 3. San Bruno, California

Site 3 is representative of sites near the San Andreas Fault, which generate strike-slip earthquakes of up to magnitude 8 along practically its entire length. Fifty-six acceleration histories derived from recordings of the M_w 7.9 2002 Denali, Alaska earthquake and broadband strong motion simulations (Graves and Pitarka, 2010) of recurrences of the M_w 7.8 1906 San Francisco earthquake (Aagaard *et al*., 2008).

3.2.2 Site 4. Berkeley, California

This site is representative of sites near the other major mapped strike slip faults in California, including the San Francisco Bay Area, the Los Angeles Region, and San Diego, which generate earthquakes of up to magnitude 7. Total of 64 acceleration histories were derived from recordings of the M_w 6.9 1989 Loma Prieta, California, M_w 6.9 1992 Erzincan, Turkey, and M_w 6.8 Tottori, Japan earthquakes.

3.2.3 Site 5. Sylmar, California

This site is representative of sites near mapped reverse and thrust faults in California, including the Los Angeles and Santa Barbara regions, which generate earthquakes of up to magnitude 7.5. A total of 56 acceleration histories were derived from recordings of the M_w 7.35, Tabas, M_w 6.9 1989 Loma Prieta, California, M_w 6.7 1994 Northridge, California, and M_w 7.6 Chi-Chi, Taiwan earthquakes.

3.3 Basin and range (Intermountain West)

The Basin and Range Province occupies a broad region extending from the coastal margin of California, Oregon and Washington to the Rocky Mountains. This region is characterized by normal and strike-slip faulting.

3.3.1 Site 6. Salt Lake City, Utah

Site 6 is representative of sites near mapped normal faults in the Basin and Range region of the Intermountain West, including the Wasatch fault near Salt Lake City, which generates earthquakes of up to magnitude 7. Fifty-six acceleration histories were derived from recordings of the 1980 M_w 6.06 Mammoth Lakes, California, 1980 M_w 6.2 Irpinia, Italy, 1980 M_w 6.9 Irpinia, Italy, and 1995 M_w 6.4 Dinar, Turkey earthquakes.

3.4 Central and Eastern United States

The Central and Eastern United States includes the region east of the Rocky Mountains. It contains only few identified faults, which are characterized by strike-slip or reverse faulting. These identified faults include the New Madrid Seismic Zone, the Meers fault, and the Cheraw fault.

3.4.1 Site 7. Cheraw, Colorado

This site is representative of sites near mapped reverse faults in Colorado (Cheraw fault) and oblique reverse faults in Oklahoma (Meers fault), which generate earthquakes of up to magnitude 7. Due to a lack of historical earthquake records, 56 acceleration histories were derived from broadband strong motion simulations of M_w 7.0 reverse faulting earthquakes at hanging wall sites for earthquakes in stable continental regions (Somerville *et al*., 2009).

3.4.2 Site 8. Tiptonville, Tennessee

Site 8 is representative of sites near mapped reverse and strike-slip faults in the New Madrid Fault Zone, which generate earthquakes of up to magnitude 7.5. A total of 48 acceleration histories were derived from broadband strong motion simulations of M_w 7.5 reverse faulting earthquakes at hanging wall sites for earthquakes in stable continental regions (Somerville *et al*., 2009).

3.4.3 Site 9. New York City, New York

This site is representative of sites near unmapped reverse faults in the Central and Eastern United States, which generates earthquakes of up to magnitude 7. A total of 56 acceleration histories were derived from broadband strong motion simulations of M_w 6.5 reverse faulting earthquakes at hanging wall sites for earthquakes in stable continental regions (Somerville *et al*., 2009).

4 Methodology to develop residual drift spectra

The program OpenSees (McKenna *et al*., 2006) was utilized to determine residual drift ratios for a range of periods and expected lateral displacement ductilities. A cantilever 0.41-m (16-in.) diameter reinforced concrete bridge column was assumed and nonlinear response history analysis with fiber elements was performed to generate residual displacement data. The column height was 1.8 m (72 in.). The axial load index, which is the ratio of the axial load to the product of the gross cross stion area and the concrete compressive strength, was 8%. The concrete compressive strength was 41.4 MPa (6 ksi). Gr. 60 steel was utilized for the longitudinal and transverse reinforcement. The transverse steel ratio was 1% and the longitudinal steel ratio changed from 1% to 4%. The fundamental period of the column was varied by keeping the mass constant but allowing variation in the column length. For each model representing a particular column period, the critical maximum displacement and residual displacement were calculated based on the response history analysis by applying FN-FP and H1-H2 components of different earthquakes to the model. The schematic analytical model is shown in Fig. 2. The cantilever column was modeled utilizing fiber force based NonlinearBeamColumn elements. The column element was divided into four equal segments with five integration points. The fiber stion was discretized into core (confined) concrete, steel fibers as longitudinal bars, and cover fibers (unconfined). Concrete01 was utilized to model unconfined concrete fibers. The confined concrete was modeled using Concrete02. To model steel fibers, ReinforcingSteel was used (McKenna *et al*., 2006). A detailed description of the analytical model is beyond the scope of the present paper and is presented elsewhere (Saiidi and Seyed Ardakani, 2012).

The following steps were used in the construction of residual drift spectra:

Step-1: Assume a column height

Step-2: Conduct pushover analysis to determine the effective yield displacement (Δ_y) and the first yield displacement corresponding to the displacement at

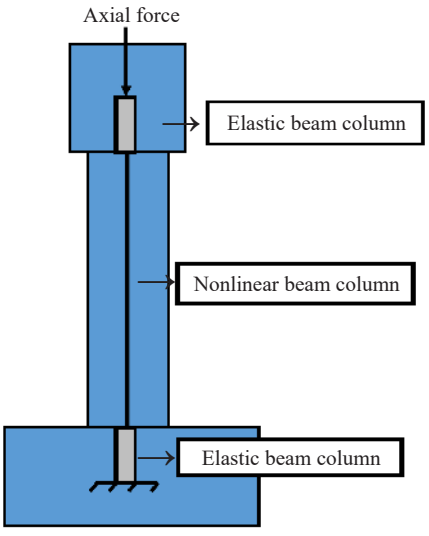

Fig. 2 Schematic analytical model

which first yield occurs in longitudinal reinforcement. The ultimate displacement (Δ_u) corresponds to the displacement at which core edge concrete reaches the ultimate compressive strain capacity. To determine the effective yield displacement (Δ_y), an elasto-plastic curve was generated using the first yield displacement and ultimate displacement by balancing the areas below and above the bilinear curve (Fig. 3). The elastic part of the idealized curve was determined by connecting the origin to the point of the first yield displacement.

Step-3: Conduct response history analysis to determine the maximum and residual displacements.

Step-4: Determine the displacement ductility demand by dividing the maximum displacement from the response history analysis by the effective yield displacement obtained from the pushover analysis.

Step-5: Draw the residual displacement versus period for the corresponding ductility demand.

Step-6: Change the column height and repeat the process from step 2.

For each model, a range of displacement ductility demands was generated by changing the confinement properties of concrete in the core. Also, the ratio of cracked to gross moment of inertia of the stion was varied: 0.3, 0.4, 0.5, 0.6, and 0.7.

5 Residual drift limit

Currently, there are no provisions to limit residual displacements in bridge columns caused by near-fault earthquakes in US bridge seismic design codes. The analysis of residual drift ratio by Saiidi and Ardakani (2012) indicated that bridge columns meeting current seismic codes are able to carry large traffic loads even when the permanent lateral drift is as high as 1.2%. A residual drift ratio limit of one percent was assumed in the present study to be more conservative. The one percent limit is the same as that specified in the bridge seismic design code of Japan (JRA, 1996). Initial analyses showed that residual drift is less than one percent when spectral acceleration at 1.0 s (S_1) is less than 0.4 g. Thus, records with one-s spectral acceleration of less than 0.4 g were ignored. These records were from site 6- Salt Lake City, Utah, site 7- Cheraw, Colorado, and site 9- New York City, New York.

6 Recorded near-fault ground motions

AASHTO LRFD Bridge Design Specifications (AASHTO, 2017) include maps for PGA, and response spectral accelerations (S_a) at 0.2 and 1.0 s. The difference between near-fault ground motions and ordinary ground motions is not significant for S_a at 0.2 s, but is significant for S_a at periods of 1.0 s and more (Somerville *et al*., 2009; Chioccarelli and Iervolino, 2010). Assuming that near-fault earthquake effects are included in the AASHTO maps, it was decided to tie the residual displacement spectrum to the spectral acceleration value at 1.0 s (S_1) because residual displacement is sensitive to near-fault effects. This allows an engineer to determine spectral accelerations for the nominally1000-year return period (which is close to 975-year return period) for the bridge location based on the AASHTO maps and then estimate the residual displacement. Tables 1 and 2 summarize the range of average PGA and S_1 for ground motions for each site, and for V_{s30} = 360 m/s (1200 ft/s) and V_{s30} = 760 m/s (2500 ft/s), respectively. Because peak ground acceleration (PGA) and one-second spectral acceleration (S_1) for different components of an acceleration history were approximately the same, an average of these parameters was used as a representative of each pair of orthogonal components (FN-FP and H1-H2). The range of average PGA and S_1 for V_{s30} = 360 m/s

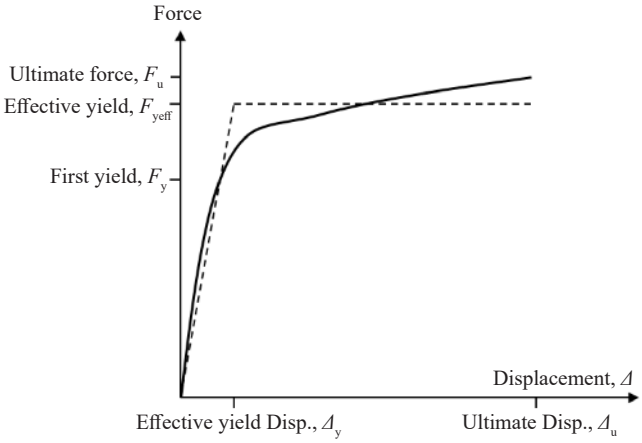

Fig. 3 Typical pushover curve for a concrete bridge column

Table 1 Range of PGA and S_1 for different sites and V_{s30} = 360 m/s (1200 ft/s)

Site	Average PGA (g)	Average S_1 (g)
Seattle	0.49–0.64	0.45–0.50
Eureka, CA	0.84–1.14	1.07–1.18
San Bruno, CA	0.84–0.94	1.07–1.16
Berkeley, CA	0.89–1.20	1.20–1.30
Sylmar, CA	0.84–1.00	1.05–1.12
Salt Lake City, UT	0.31–0.38	0.35–0.38
Cheraw, CO	0.04–0.05	0.4
Tiptonville, TN	1.02–1.17	0.67–0.74
New York City, NY	0.09–0.11	0.05

Table 2 Range of PGA and S_1 for different sites and V_{s30} = 760 m/s (2500 ft/s)

Site	Average PGA (g)	Average S_1 (g)
Seattle	0.36–0.50	0.29–0.32
Eureka, CA	0.78–1.15	0.67–0.71
San Bruno, CA	0.73–0.89	0.63–0.78
Berkeley, CA	0.80–1.13	0.73–0.79
Sylmar, CA	0.81–1.05	0.62–0.70
Salt Lake City, UT	0.28–0.32	0.21–0.23
Cheraw, CO	0.03–0.04	0.02–0.03
Tiptonville, TN	1.04–1.12	0.54–0.61
New York City, NY	0.07–0.08	0.03

Table 3 Number of records

S_1 (g)	V_{s30} = 360 m/s (1200 ft/s)	V_{s30} = 760 m/s (2500 ft/s)
0.4–0.6	14	13
0.6–0.8	14	57
> 0.8	60	0

(1200 ft/s) is higher than that for V_{s30} = 760 m/s (2500 ft/s), which is attributed to the higher amplification effects for V_{s30} = 360 m/s (1200 ft/s) due to the soil site compared to the rock site for V_{s30} = 760 m/s (2500 ft/s).

Three ranges of spectral acceleration associated with fundamental period of 1.0 s (S_1) were assumed: 1) 0.4–0.6 g, 2) 0.6–0.8 g, and 3) > 0.8 g. Two shear wave velocities were assumed for each range: V_{s30} = 360 m/s (1200 ft/s) and V_{s30} = 760 m/s (2500 ft/s). Table 3 shows the number of records for each case. While there is a large number of records for each range of S_1 for V_{s30} = 360 m/s (1200 ft/s), there is no record for the range of S_1 > 0.8 g for V_{s30} = 760 m/s (2500 ft/s). This is expected because for V_{s30} = 760 m/s (2500 ft/s) the acceleration histories are on the rock and very stiff sites. As a result, compared to V_{s30} = 360 m/s (1200 ft/s), there is considerably less amplification in the spectrum especially at higher periods leading to few sites having S_1 exceeding 0.8 g.

To fill the gap in the earthquake records for the range of S_1 > 0.8 g with shear wave velocity of V_{s30} = 760 m/s (2500 ft/s) recorded near-fault ground motions were obtained from the Pacific Earthquake Engineering Research (PEER) Center website. Three criteria were applied to selecting the ground motions: (1) the earthquake magnitude is 6.5 or higher, (2) the site is within 15 km (9 miles) of the fault, and (3) 540 m/s (1800 ft/s) ≤ V_{s30} ≤ 760 m/s (2500 ft/s). Seven records were identified. The major principal component was used to represent motion in the fault-normal direction and the minor principal component was used to represent motion in the fault-parallel direction. The recorded near-fault ground motions and their characteristics are presented in Table 4.

7 Residual drift spectra

Residual drifts were determined for maximum displacement ductilities of 2, 4, and 6. Because the scatter in residual drift was relatively high, it was decided that for each period and ductility demand, residual drift response spectra be constructed for the average, average plus one standard deviation and average minus one standard deviation.

The period ranged from 0.1 to 2.0 s with increments of 0.05 s. For each period and ductility value, a residual

Table 4 Recorded near-fault ground motions

Earthquake	Station	Magnitude	Distance (km) (mi)	V_{s30} (m/s) (ft/s)	S_1 (g) (Avg.)
Chi-Chi	CHY028	7.6	7.31 (4.38)	543 (1810)	1.04
Chi-Chi	CHY080	7.6	6.95 (4.16)	680 (2267)	2.09
Chi-Chi	TCU052	7.6	0.24 (0.14)	579 (1930)	0.99
Chi-Chi	TCU074	7.6	13.67 (8.19)	549 (1830)	1.1
Chi-Chi	TCU084	7.6	10.39 (6.22)	680 (2267)	1.7
Northridge	Pacoima Dam (upper left)	6.7	8.00 (4.79)	2016 (6720)	0.84
San Fernando	Pacoima Dam	6.6	2.80 (1.68)	2016 (6720)	0.98

drift response spectrum for each S_1 and site condition combination was generated.

7.1 Residual drift spectra for cracked stiffness ratio of 0.5

Figure 4 shows the residual drift spectra for ductility of two for all ground motions with V_{s30} = 360 m/s (1200 ft/s) and S_1: 0.4–0.6 g. The ratio of the cracked to the gross moment of inertia of the stion was 0.5. As can be seen, the spectra include distinct valleys as column period increases. This is due to the effective period of the column as it relates to the frequency content of the ground motion. It was felt that the envelope of the residual drift spectra would be a more reasonable representative set of curves for use in design. The envelopes of residual drift response spectra for the average and average plus one standard deviation are shown in Fig. 5. To be more conservative, the envelopes of residual drift response spectra for the average minus one standard deviation were not generated. The envelopes eliminate the valleys in the curves of Fig. 4 and present a more conservative estimate of the residual drift ratios for the period ranges where the valleys occur. Figures 6 to 10 present the envelope of residual drift spectra for different V_{s30}, ductility, and ranges of S_1. Figure 6(a) shows the residual drift spectra for V_{s30} = 360 m/s (1200 ft/s), ductility of two, and S_1 range of 0.6–0.8 g. Compared to Fig. 5, higher residual drifts are obtained because of the higher intensity of S_1. For an effective period of 1.0 s, the estimated residual drift ratio based on the average and average plus one standard deviation is approximately 0.55% and 0.75%, respectively.

Residual drift spectra for V_{s30} = 360 m/s (1200 ft/s), ductility of four, and S_1: 0.6–0.8 g is shown in Fig. 6(b). As the maximum displacement ductility demand increases, the residual drift significantly increases. The residual drift exceeds 1% when the column period is greater than approximately 0.50 s and 0.45 s for the average and average plus standard deviation plots, respectively. As S_1 increases, the residual drift becomes greater (Fig. 7). While the residual drift for the average plus standard deviation plot is less than 1% for S_1 of 0.6-0.8 g and ductility of two (Fig. 6(a)), it exceeds 1% for the same ductility and S_1 > 0.8 g (Fig. 7(a)) for the period of approximately 0.90 s and 0.55 s and higher for the average and average plus one standard deviation plots, respectively. This is attributed to the stronger input earthquakes for this range of S_1.

Another important trend is that as the maximum displacement ductility demand increases, the residual drift ratio increases (Figs. 6 and 7), as expected. According to Fig. 7(b) for ductility of four, the residual drift exceeds 1% for periods exceeding 0.40 and 0.25 s for the average and average plus standard deviation plots, respectively. The corresponding periods based on Fig. 7(c) for ductility of six are 0.3 and 0.2 s, which means that columns subjected to high displacement ductility

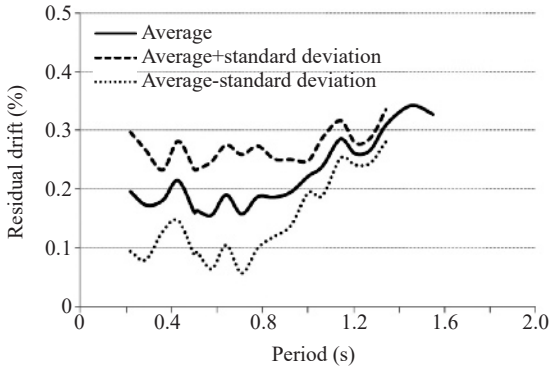

Fig. 4 Residual drift spectra for V_{s30} = 360 m/s (1200 ft/s), ductility of two, and S_1: 0.4 g–0.6 g

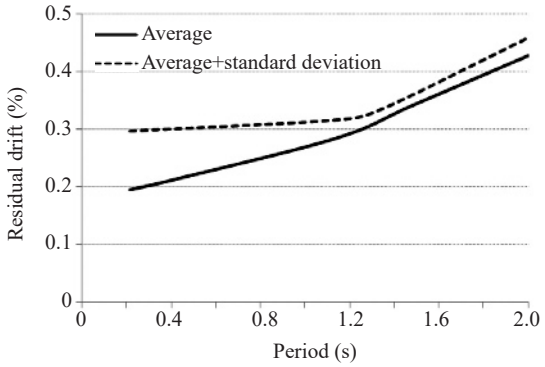

Fig. 5 Residual drift spectra envelope for V_{s30} = 360 m/s (1200 ft/s), ductility of two, and S_1: 0.4 g–0.6 g

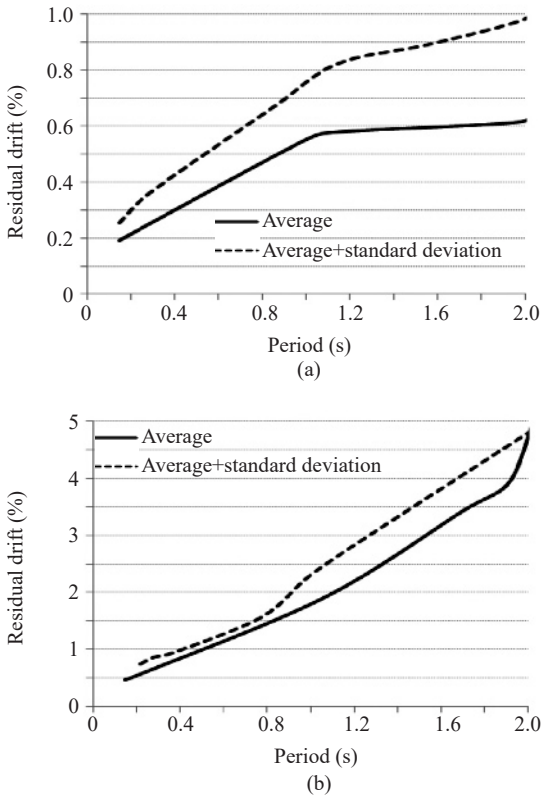

Fig. 6 Residual drift spectra envelope for V_{s30} = 360 m/s (1200 ft/s), S_1: 0.6 g–0.8 g, ductility of a) two and b) four

demands must be designed for near-fault ground motion effects. For V_{s30} = 760 m/s (2500 ft/s), the corresponding plots are presented in Figs. 8 to 10. A similar trend can be seen for this site condition; however, the residual drift is generally lower because of the smaller amplification of ground motion on stiff soil compared to softer sites.

7.2 Residual drift spectra for cracked stiffness ratio of 0.3, 0.4, 0.6, and 0.7

Since the effective stiffness of cracked reinforced concrete stions could generally vary from 0.3 to 0.7 of the gross moment of inertia (Caltrans, 2013), the residual drift spectra for ratios of 0.3, 0.4, 0.6, and 0.7 were also generated. The envelopes of residual drift spectra for the average and average plus one standard deviation corresponding to these ratios for both site conditions are shown in Figs. 11 to 22. The trends in these figures are comparable to those for the ratio of cracked to gross moment of inertia of 0.5. The residual drift ratio becomes greater as the ratio of the cracked stion stiffness increases, which is expected. The residual drift spectra for different ranges of S_1 are described as follows.

7.2.1 S_1: 0.4–0.6 g

For S_1 of 0.4–0.6 g only the displacement ductility demand of two was generated because the energy in

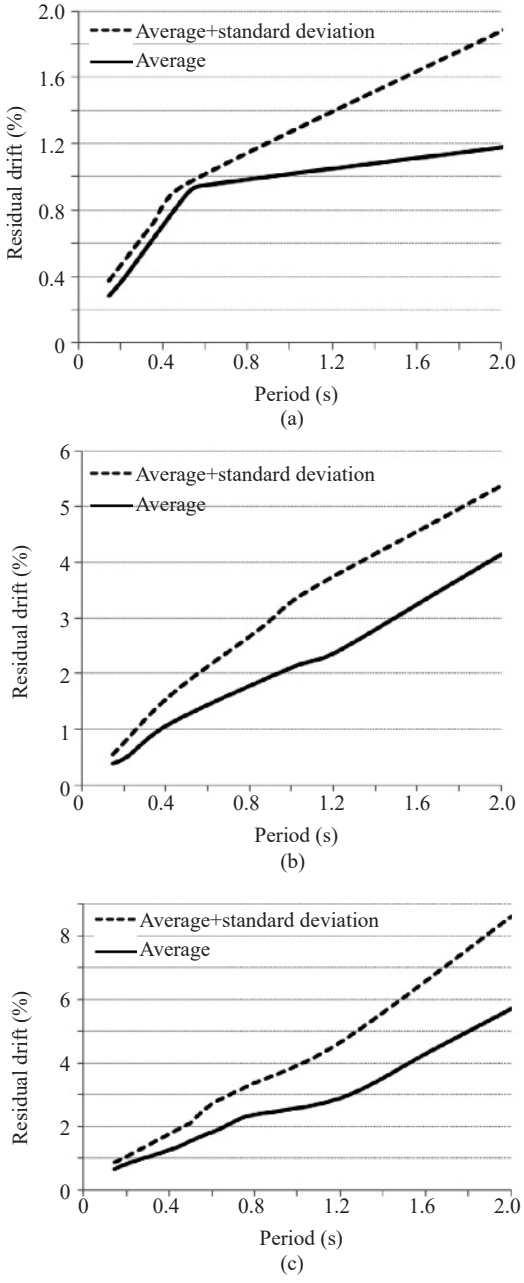

Fig. 7 Residual drift spectra envelope for V_{s30} = 360 m/s (1200 ft/s), S_1 > 0.8 g, ductility of a) two, b) four, and c) six

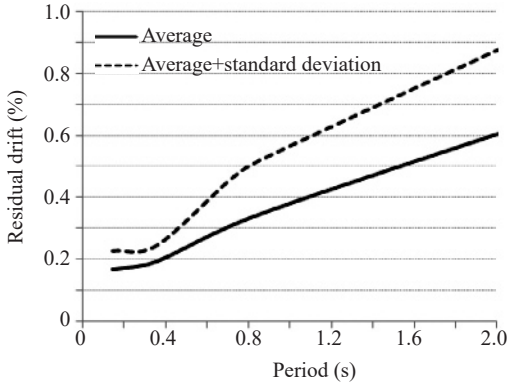

Fig. 8 Residual drift spectra envelope for V_{s30} = 760 m/s (2500 ft/s), S_1 : 0.4 g–0.6 g, ductility of two

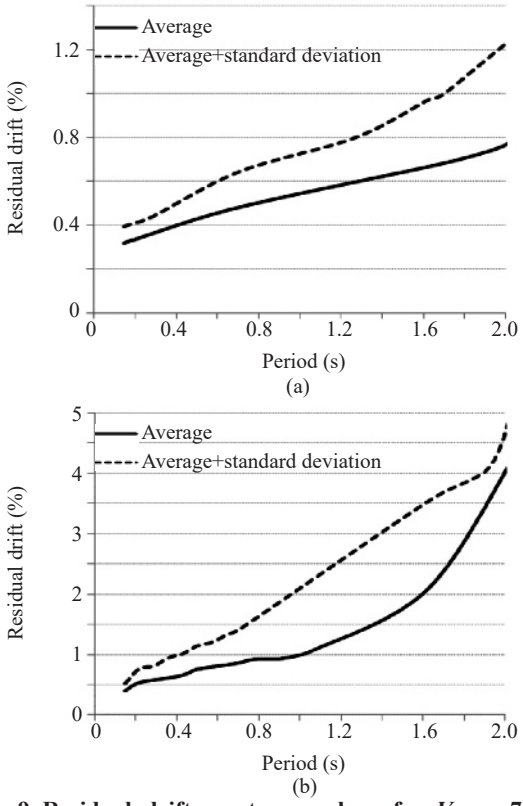

Fig. 9 Residual drift spectra envelope for V_{s30} = 760 m/s (2500 ft/s), S_1: 0.6–0.8 g, ductility of a) two and b) four

these records is not sufficiently large to place higher displacement ductilities. Also, as seen in Figs. 11 and 12, the residual drift ratio for the average and average plus standard deviation is below 1% regardless of the cracked stiffness ratio for both site conditions. For a column with a period of 0.5 s, which represents a relatively stiff column, as the cracked stiffness ratio increases from 0.3 to 0.7, the residual drift ratio increases from approximately 0.21% to 0.25% for the average while remains at approximately 0.3% for the average plus standard deviation in soil sites (Fig. 11). For the same column in the rock site based on Fig. 12, the residual drift ratio increases from approximately 0.2% to 0.3% and 0.25% to 0.40% for the average and average plus standard deviation, respectively. For a more flexible column with a period of 1.0 s in the soil site, the residual drift ratio increases from approximately 0.25% to 0.30% for the average while remains at approximately 0.3%

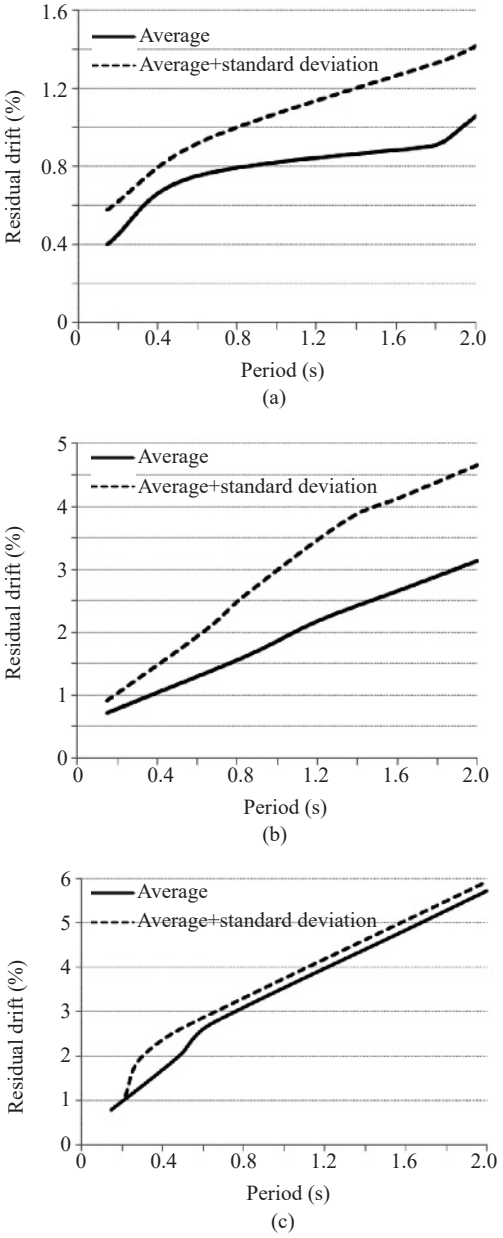

Fig. 10 Residual drift spectra envelope for V_{s30} = 760 m/s (2500 ft/s), S_1 > 0.8 g, ductility of a) two, b) four, and c) six

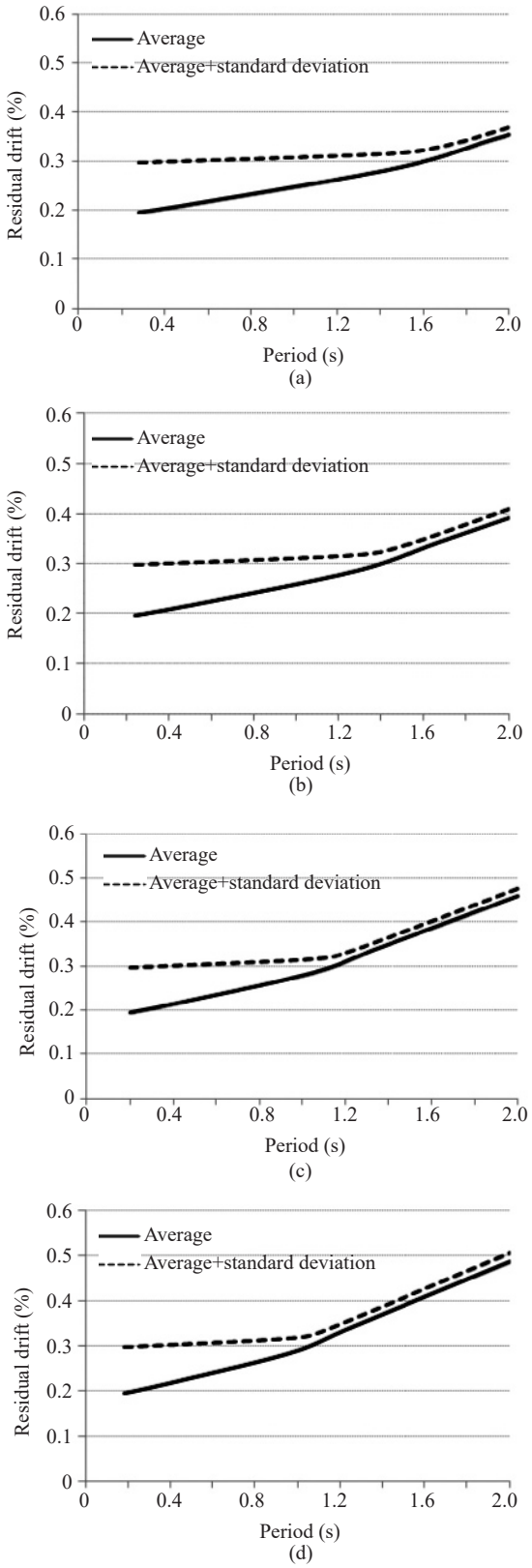

Fig. 11 Residual drift spectra envelope for V_{s30} = 360 m/s (1200 ft/s), ductility of two, S_1: 0.4–0.6 g, cracked stiffness ratio of a) 0.3, b) 0.4, c) 0.6, and d) 0.7

for the average plus standard deviation. The increase in residual displacement for the column in the rock site is from approximately 0.3% to 0.4% and 0.5% to 0.6% for the average and average plus standard deviation, respectively. For a flexible column with a period of 1.5 s in the soil site, the residual drift ratio of the column increases from approximately 0.3% to 0.4% for the average and average plus standard deviation. The residual drift ratio for this column in the rock site increases from 0.40% to 0.55% and 0.6% to 0.8% for the average and average plus standard deviation, respectively. This indicates that the residual drift ratio becomes significantly greater as the column period increases, which is attributed to the proximity of the period of the motions to the column period and consequently the higher energy input of near-fault ground motions.

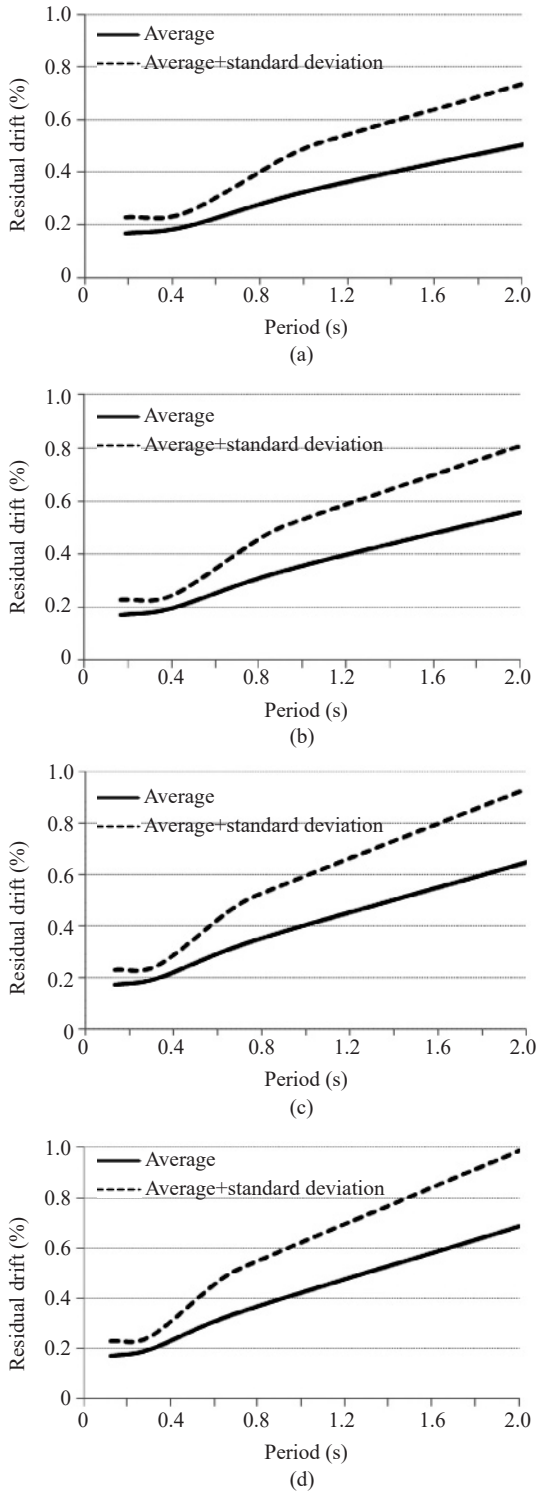

Fig. 12 Residual drift spectra envelope for V_{s30} = 760 m/s (2500 ft/s), ductility of two, S_1: 0.4–0.6 g, cracked stiffness ratio of a) 0.3, b) 0.4, c) 0.6, and d) 0.7

7.2.2 S_1: 0.6–0.8 g

For S_1 of 0.6–0.8 g, columns undergo displacement ductility demand of four as well. Based on Figs. 13 and 14, the residual drift ratio for the average data is below 1% for ductility of two regardless of the cracked stiffness ratios and the site type. However, for the average plus standard deviation, the residual drift ratio exceeds 1% when at least 60% and 40% of the stion is cracked for V_{s30} = 360 m/s (1200 ft/s) and V_{s30} = 760 m/s (2500 ft/s), respectively. Based on Fig. 13 for V_{s30} = 360 m/s (1200 ft/s) the residual drift ratio exceeds 1% at periods of 1.6 s and 1.4 s for the cracked stiffness ratios of 0.6 and 0.7, respectively. Per Fig. 14, for V_{s30} = 760 m/s (2500 ft/s), the residual drift ratio exceeds 1% as the column period exceeds 1.9 s. for the cracked stiffness ratio of 0.4. As the cracked stiffness ratio increases, the required column period to exceed the residual drift limit of 1% reduces. For a cracked stiffness ratio of 0.7, the corresponding column period is 1.4 s. For this stiffness ratio, the residual drift ratio reaches to 1.4% for a column period of 2.0 s. Figure 13 shows that for a column with a period of 0.5 s in the soil site as the cracked stiffness ratio increases, the residual drift ratio increases from approximately 0.3% to 0.4% and 0.4% to 0.6% for the average and average plus standard deviation, respectively. For the same column located on a rock site, the residual drift ratio increases from approximately 0.40% to 0.45% and 0.5% to 0.6% for the average and average plus standard deviation, respectively, (Fig. 14). Figure 13 shows that in the soil site, the residual drift ratio for a softened column with a period of 1.0 s increases from approximately 0.5% to 0.6% and 0.6% to 0.8% for the average and average plus standard deviation, respectively. The increase in residual drift ratio for this column in the rock site is from approximately 0.5% to 0.6% and 0.7% to 0.8% for the average and average plus standard deviation, respectively, as seen in Fig. 14. Per Fig. 13 for a column with a period of 1.5 s in the soil site, the residual drift ratio remains at 0.6% for the average and increases from 0.8% to 1.1% for the average plus standard deviation. Based on Fig. 14, the residual drift ratio in the column increases from 0.6% to 0.7% and 0.8% to 1.1% for the average and average plus standard deviation, respectively. This also indicates that the residual drift ratio becomes significantly greater as the column period increases. Figure 15 shows that the residual drift ratio is at least 1% for nearly all periods regardless of the cracked stiffness ratio in a soil site when the ductility demand is four. Based on Fig. 16,

for the rock site, the residual drift ratio for the average data exceeds 1% at a period of 1.0 and 0.7 s when 40% and 70% of the stion is cracked, respectively. For the average plus standard deviation data, the corresponding periods are 0.5 and 0.3 s. Per Fig. 15 for a column with a period of 0.5 s in a bridge in a soil site, the residual drift ratio is approximately 1% for all cracked stiffness ratios. For a column with a period of 1.0 s, the residual drift ratio increases to 1.5% and 2.0% for the average data as the cracked stiffness ratio increases from 0.3 to

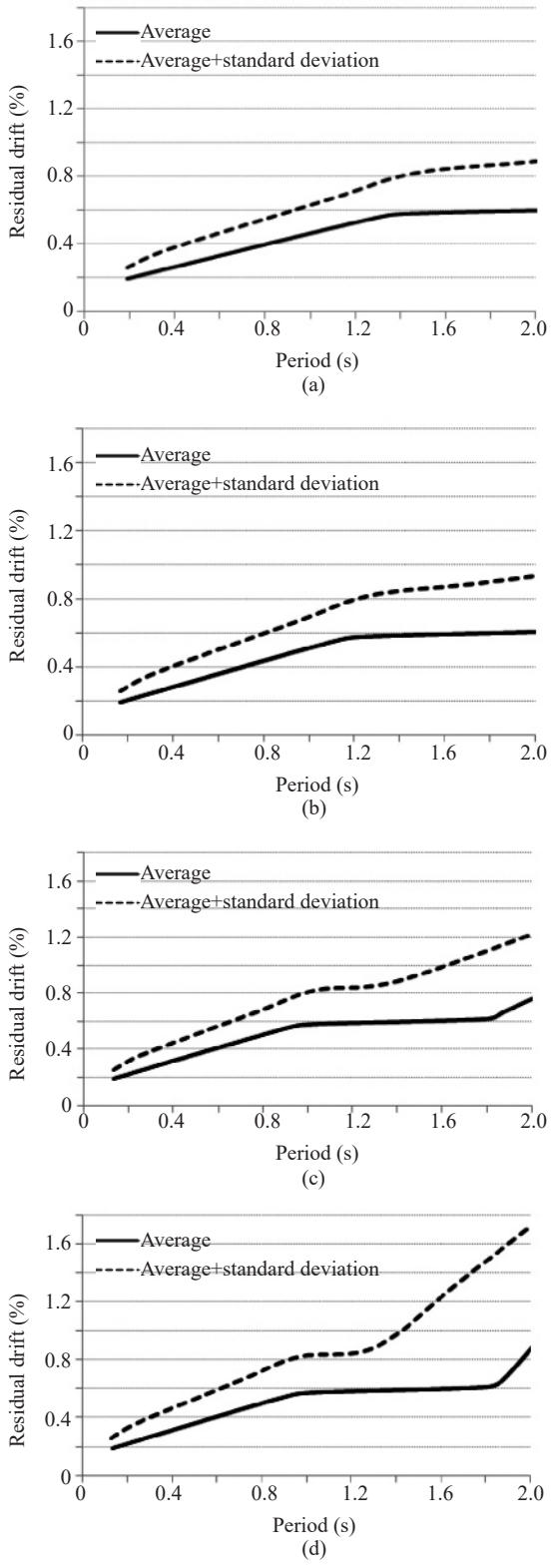

Fig. 13 Residual drift spectra envelope for V_{s30} = 360 m/s (1200 ft/s), ductility of two, S_1: 0.6–0.8 g, cracked stiffness ratio of a) 0.3, b) 0.4, c) 0.6, and d) 0.7

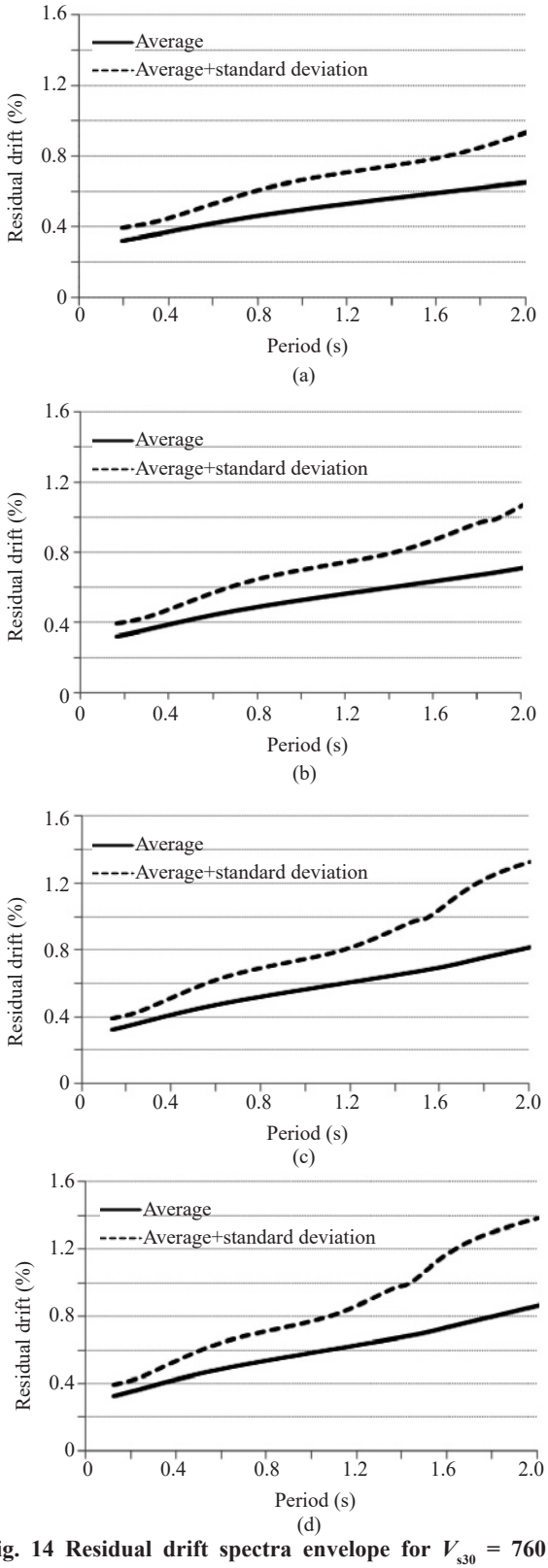

Fig. 14 Residual drift spectra envelope for V_{s30} = 760 m/s (2500 ft/s), ductility of two, S_1: 0.6–0.8 g, cracked stiffness ratio of a) 0.3, b) 0.4, c) 0.6, and d) 0.7

0.7. The increase is from 1.5% to 2.5% for the average plus standard deviation data. Figure 15 shows that for a column with a period of 1.5 s, the residual drift ratio increases from 2% to 3.5% and 3% to 5% for the average and average plus standard deviation, respectively, when the cracked stiffness ratio increases from 0.3 to 0.7. As seen in Fig. 16, for a column with a period of 0.5 s in the rock site, the corresponding residual drift ratio increase is from 0.6% to 0.9% and 1.0% to 1.5% for the average and average plus standard deviation, respectively. The corresponding increase for a column with a period of 1.0 s is from 1.0% to 1.3% and 1.6% to 2.5% for the average

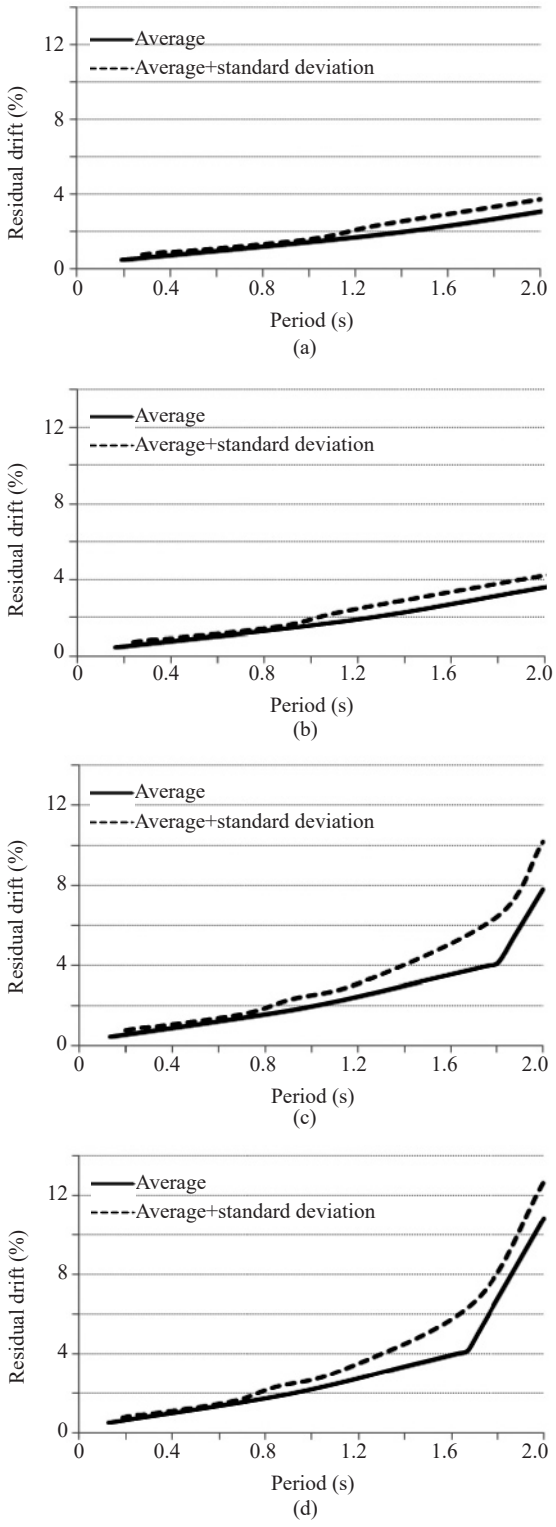

Fig. 15 Residual drift spectra envelope for V_{s30} = 360 m/s (1200 ft/s), ductility of two, S_1: 0.6–0.8 g, cracked stiffness ratio of a) 0.3, b) 0.4, c) 0.6, and d) 0.7

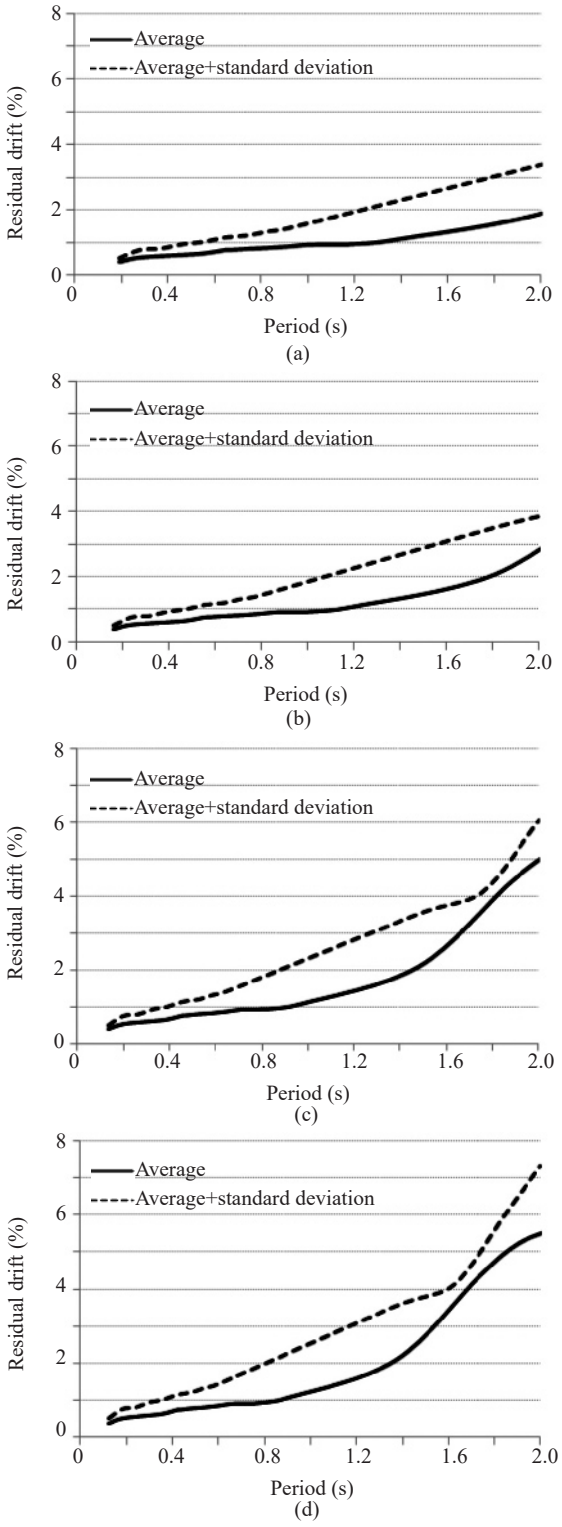

Fig. 16 Residual drift spectra envelope for V_{s30} = 760 m/s (2500 ft/s), ductility of two, S_1: 0.6–0.8 g, cracked stiffness ratio of a) 0.3, b) 0.4, c) 0.6, and d) 0.7

and average plus standard deviation, respectively. The corresponding increases for a column with a period of 1.5 s are from 1.2% to 2.5% and 2.5% to 3.8%. This indicates that as the ductility demand increases, the residual drift ratio drastically becomes greater for long-period columns.

7.2.3 S_1: > 0.8 g

For S_1 > 0.8 g ductility demands of two, four, and six are generated in the columns. Figure 17 shows that

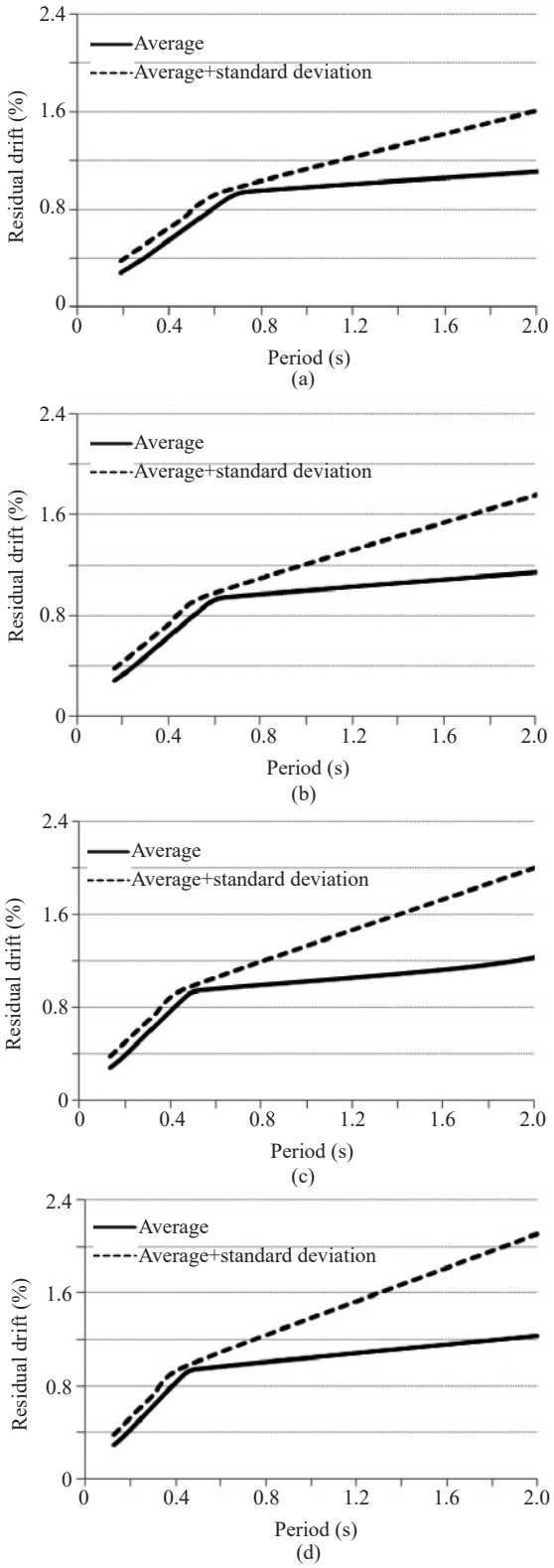

Fig. 17 Residual drift spectra envelope for V_{s30} = 360 m/s (1200 ft/s), ductility of two, S_1: > 0.8 g, cracked stiffness ratio of a) 0.3, b) 0.4, c) 0.6, and d) 0.7

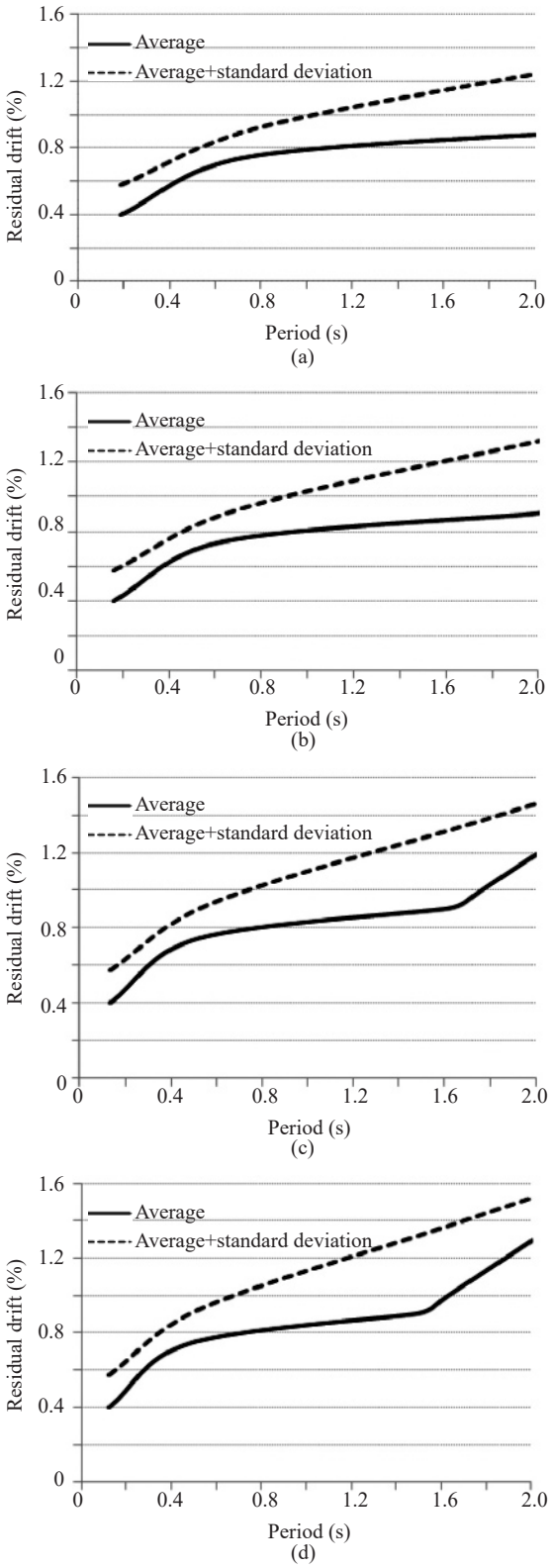

Fig. 18 Residual drift spectra envelope for V_{s30} = 760 m/s (2500 ft/s), ductility of two, S_1: > 0.8 g, cracked stiffness ratio of a) 0.3, b) 0.4, c) 0.6, and d) 0.7

the residual drift ratio of a column in the soil site that undergoes ductility demand of two exceeds 1% for the average data as the period exceeds 1.0 and 0.7 s for a cracked stiffness ratio of 0.3 and 0.7, respectively. The corresponding periods for the average plus standard deviation data are 0.7 and 0.5 s. Based on Fig. 18, the residual drift ratio of a column in the rock site is less than 1% for the average data when the cracked stiffness ratio is less than 0.5. Additionally, the residual drift ratio for the average data exceeds 1% as the column period

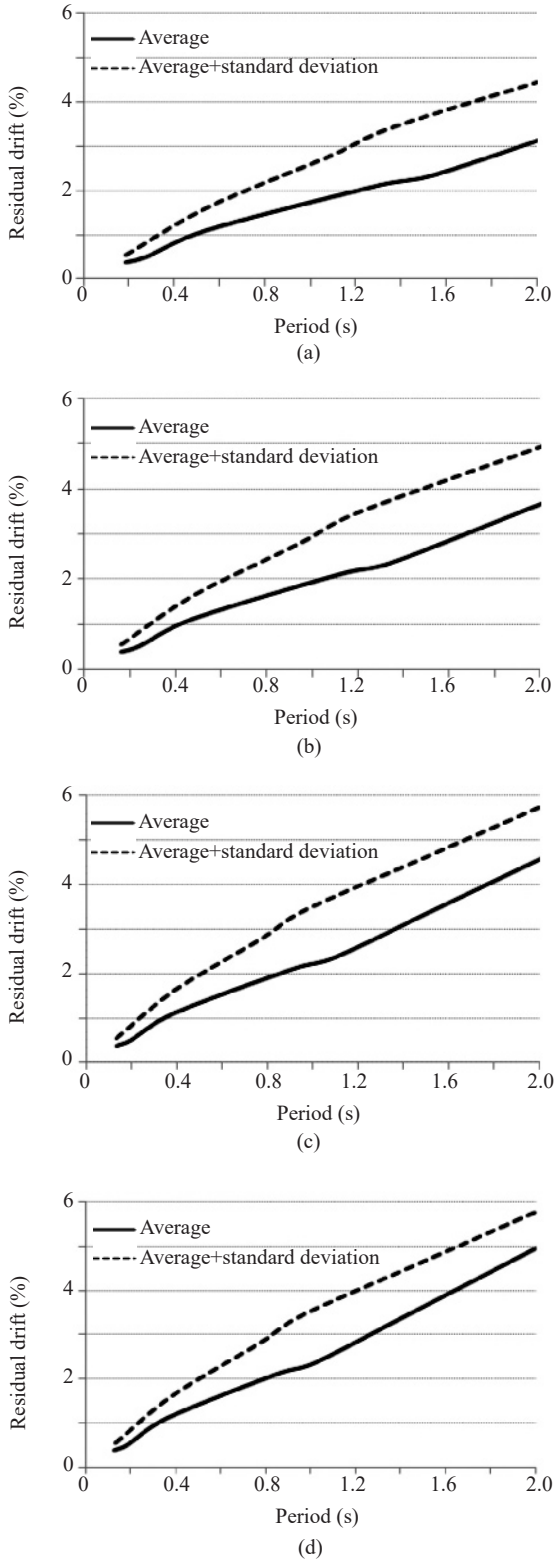

Fig. 19 Residual drift spectra envelope for V_{s30} = 360 m/s (1200 ft/s), ductility of four, S_1: > 0.8 g, cracked stiffness ratio of a) 0.3, b) 0.4, c) 0.6, and d) 0.7

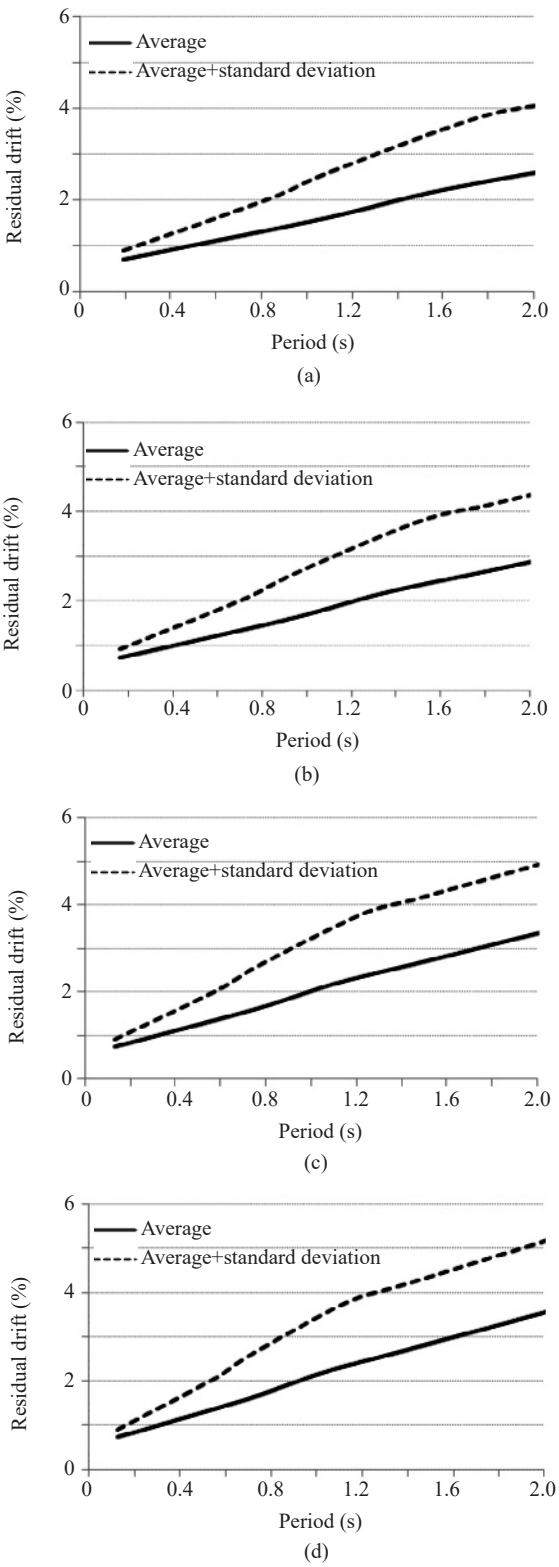

Fig. 20 Residual drift spectra envelope for V_{s30} = 760 m/s (2500 ft/s), ductility of four, S_1: > 0.8 g, cracked stiffness ratio of a) 0.3, b) 0.4, c) 0.6, and d) 0.7

exceeds 1.8 and 1.6 s for cracked stiffness ratios of 0.6 and 0.7, respectively. For the average plus standard deviation data, the residual drift ratio exceeds 1% as the column period exceeds 1.1 and 0.7 s for cracked stiffness ratios of 0.3 and 0.7, respectively. Figure 17 shows that for a column with a period of 0.5 s in the soil site, the residual drift ratio increases from 0.7% to approximately 1.0% and 0.8% to 1.1% for the average and average plus standard deviation, respectively, when the cracked stiffness ratio increases from 0.3 to 0.7. The corresponding increase in the residual drift ratio of the column in the rock site per Fig. 18 is from 0.7% to 0.8% and 0.8% to 0.9% for the average and average plus standard deviation, respectively. For a column with a period of 1.0 s in the soil site (Fig. 17), the residual drift ratio increases from 1.0% to 1.1% and 1.2% to 1.4% for the average and average plus standard deviation, respectively, as the cracked stiffness ratio increases from 0.3 to 0.7. The corresponding increase in the residual displacement for the column is the rock site is from 1.0% to approximately 1.2% for the average plus standard deviation, but remains at approximately 0.8% for the average data. Figure 17 shows that for a column with a period of 1.5 s in the soil site, the residual drift ratio increases from approximately 1.0% to 1.2% and 1.4% to 1.7% for the average and average plus standard deviation, respectively, with the increase of the cracked stiffness ratio from 0.3 to 0.7. Based on Fig. 18, the corresponding increases for the column in the rock site are from approximately 0.8% to 0.9% and 1.1% to 1.3% for the average and average plus standard deviation, respectively. This indicates that the design engineer must be extremely cautious during the design process since as the longitudinal steel ratio and consequently the effective stiffness of a column varies, the residual drift ratio may exceed 1%. Figures 19 and 20 present the residual drift spectra for a column with a displacement ductility demand of four when $S_1 > 0.8$ g for soil and rock sites, respectively. Figure 19 shows that the residual drift ratio exceeds 1% for the average data when the column period is more than 0.5 and 0.3 s for cracked stiffness ratios of 0.3 and 0.7, respectively. For the average plus standard deviation data, the corresponding periods are approximately 0.3 and 0.2 s. Per Fig. 20 for the rock site, the residual drift ratio for a cracked stiffness ratio of 0.3 exceeds 1% at periods of approximately 0.4 and 0.2 s for the average and average plus standard deviation, respectively. The corresponding periods for a cracked stiffness ratio of 0.7 are approximately 0.30 and 0.15 s for the average and average plus standard deviation, respectively. For a column with a period of 0.5 s and cracked stiffness ratio of 0.3 in the soil site, the residual drift ratio is 1% and 1.5% for the average and average plus standard deviation data, respectively. As the cracked stiffness ratio increases to 0.7, the residual drift ratio increases to 1.5% and 2.0% for the average and average plus standard deviation data, respectively. For the rock site, as seen in Fig. 20, the residual drift ratio in the column increases from 1.0% to 1.3% and 1.5% to 2.0% for the average and average plus standard deviation, respectively, as the cracked stiffness ratio increases from 0.3 to 0.7. For a column with a period of 1.0 s in the soil site per Fig. 19, the residual drift ratio increases from 1.7% to 2.2% and 2.5% to 3.5% for the average and average plus standard deviation, respectively. The corresponding increase in the residual drift ratio for the column in the rock site is from 1.5% to 2.1% and 2.4% to 3.5% for the average and average plus standard deviation, respectively. The values for a column with a period of 1.5 s in the soil site per Fig. 19 are 2.2% to 3.5% and 3.6% to 4.5% for the average and average plus standard deviation, respectively. Based on Fig. 20, this column in the rock site undergoes a residual drift ratio of 2.0% and 3.5% for the average and average plus standard deviation, respectively, when the cracked stiffness ratio is 0.3. As the cracked stiffness ratio increases to 0.7, the corresponding residual drift ratios are 2.9% and 4.5%. The residual drift spectra for $S_1 > 0.8$ g and ductility demand of six are presented in Figs. 21 and 22 for soil and rock sites, respectively. For both sites, the residual drift ratio exceeds 1% for all periods for the average plus standard deviation data. For the average data, the residual drift ratio exceeds 1% at approximately 0.3 and 0.2 s for soil and rock sites, respectively. Based on Fig. 21, for a column with a cracked stiffness ratio of 0.3 and a period of 0.5 s in the soil site, the residual drift ratios are 1.2% and 1.9% for the average and average plus standard deviation, respectively. As the cracked stiffness ratio increases, the residual drift ratio becomes greater as well. For the cracked stiffness ratio of 0.7, the corresponding residual drift ratios are 2.0% and 2.5%. For the column in the rock site with a cracked stiffness ratio of 0.3, as seen in Fig. 22, the residual drift ratios are approximately 1.9% and 2.5% for the average and average plus standard deviation, respectively. The corresponding residual drift ratios increase to 2.6% and 2.9% for the cracked stiffness ratio of 0.7. Figure 21 shows that for a column with a period of 1.0 s and cracked stiffness ratio of 0.3 in a site with $V_{s30} = 360$ m/s (1200 ft/s), the residual drift ratio is approximately 2.2% and 3.2% for the average and average plus standard deviation, respectively. The corresponding values for the cracked stiffness ratio of 0.7 are 2.9% and 4.0%. For $V_{s30} =$ 760 m/s (2500 ft/s) based on Fig. 22, the residual drift ratio increases from 3.2% and 3.3% to 4.0% and 4.1% for the average and average plus standard deviation, respectively, as the cracked stiffness ratio increases from 0.3 to 0.7. Per Fig. 21, a column with a period of 1.5 s and a cracked stiffness ratio of 0.3 in the soil site undergoes a residual drift ratio of 3.0% and 4.5% for the average and average plus standard deviation, respectively. As the cracked stiffness ratio increases to 0.7, the corresponding residual drift ratios increase to 5% and 7%. As seen in Fig. 22, the column in the rock site undergoes a residual

drift ratio of 4.2% and 4.5% for the average and average plus standard deviation, respectively, when the cracked stiffness ratio is 0.3. The corresponding ratios increase to 5.1% and 5.5% as the cracked stiffness ratio increases to 0.7.

8 Evaluation of residual drift spectra

In studies by Phan *et al*. (2007) and Choi *et al*. (2010), six large-scale reinforced concrete bridge columns were tested in the Large Scale Structures Laboratory at the University of Nevada, Reno. The columns were

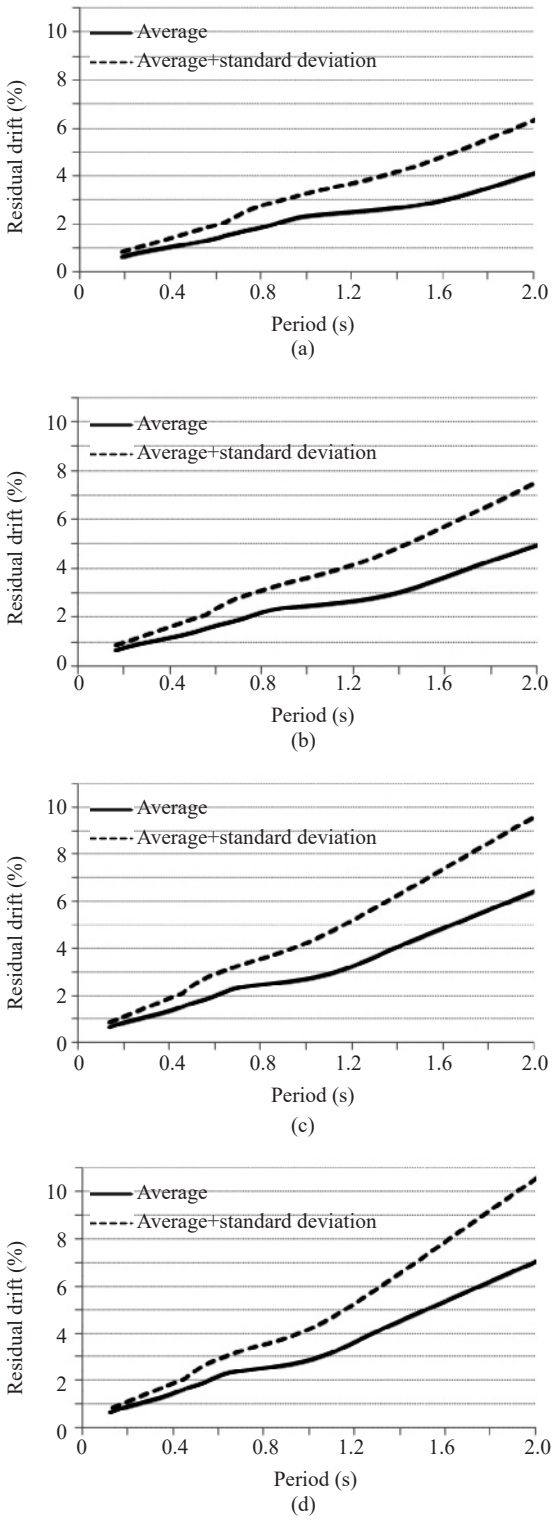

Fig. 21 Residual drift spectra envelope for V_{s30} = 360 m/s (1200 ft/s), ductility of six, S_1: > 0.8 g, cracked stiffness ratio of a) 0.3, b) 0.4, c) 0.6, and d) 0.7

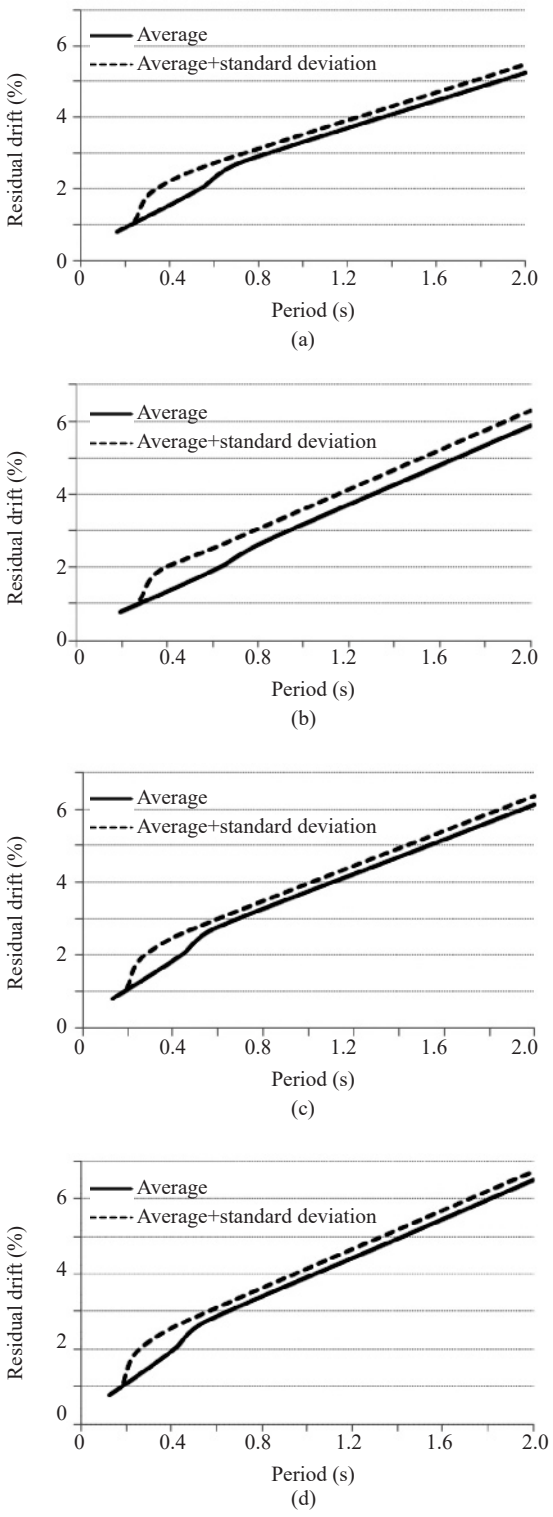

Fig. 22 Residual drift spectra envelope for V_{s30} = 760 m/s (2500 ft/s), ductility of six, S_1: > 0.8 g, cracked stiffness ratio of a) 0.3, b) 0.4, c) 0.6, and d) 0.7

Table 5 Measured and calculated residual drift ratio for different columns

Column	Run	Period (s)	Ductility demand	Cracked stiffness ratio	S_1 (g)	V_{s30} (m/s) (ft/s)	Measured Residual drift ratio, RDR (%)	Calculated RDR per average spectra (%)	Calculated RDR per average pus standard deviation spectra (%)
NF-1	9	1.6	8	0.9	1.3	282 (930)	5.9	5.2	8
NF-2	9	1.4	8	0.9	1.3	282 (930)	4	4.5	6.5
MN	9	1.1	9	0.9	1.3	282 (930)	4.3	3	4.5
ETN	9	1.3	2	0.7	1.3	282 (930)	0.1	1.1	1.6
SETN	9	1.9	5	0.9	1.3	282 (930)	6.9	5.5	7.8
SVTN	9	1.5	4	0.8	1.3	282 (930)	1	3.5	4.5
UCSD	3	2	5	0.7	0.7	478 (1550)	0.9	9.3	10.7
UCSD	5	2.6	8	0.8	1.3	312 (1000)	1.4	7	10.5
UCSD	6	2.4	7	0.8	0.7	478 (1550)	0.7	9.3	10.7

all flexure-dominated circular spiral columns tested as cantilever members. The specimens were labeled NF-1, NF-2, MN, ETN, SETN, and SVTN. The design of NF-1 was according to the 2004 Caltrans Seismic Design Criteria (Caltrans, 2004), but did not incorporate Caltrans near-fault guidelines. The design of NF-2 was based on the AASHTO 2002 Standard Specifications for Highway Bridges. The MN was similar to NF-1, but accounted for Caltrans near-fault guidelines. The difference between MN and ETN was the initial cracked stiffness period of the columns. SETN was comparable to ETN; however, spectral acceleration for SETN was determined from a new design spectrum by Somerville. The new spectrum presented higher spectral accelerations at the period of 1.25 s or higher compared to the Caltrans near-fault spectrum (Choi *et al*., 2007). SVTN was designed as a long-period column based on the new design spectrum. The fault normal component of the Rinaldi ground motion from the 1994 Northridge Earthquake was applied in NF-1, NF-2, MN, and ETN. SETN and SVTN were tested using the Rinaldi Receiving Station (RRS) record. The RRS record was a synthetic motion generated by matching in the frequency domain the Rinaldi motion to the new spectrum developed by Somerville. All columns were tested under small amplitude motions followed by motions with gradually increasing amplitudes from one motion to the next until the column failed or shake table testing limits were reached. Measured data for these specimens were utilized to evaluate the residual drift spectra in the present study. Since the columns were subjected to the full amplitude motion of the records (either 1.05xRinaldi or 1.05xRRS) during Run 9, the measured data for other runs were excluded from the study. In addition, measured data from shake table testing of a full-scale column tested at the University of California, San Diego (UCSD) were included in the study (Terzic *et al*., 2015). This model is referred to as "UCSD column" in this article. The column was a flexure-dominated circular reinforced concrete bridge column tested as a cantilever member. The design of the column was based on the 2006 Caltrans Seismic Design Criteria (Caltrans, 2006) and the 2004 Caltrans Bridge Design Specifications (Caltrans, 2004). The specimen was subjected to six far-field and near-field ground motions recorded at Agnews State Hospital (Run 1), Corralitos (Runs 2 & 4), LGPC (Runs 3 & 6) stations during the 1989 Loma Prieta earthquake, and Takatori station (Run 5) during the 1995 Kobe earthquake. The ground motions at Agnews State Hospital and Corralitos from the Loma Prieta earthquake are far-field motions because the records do not contain high-velocity pulses. Table 5 lists the measured and calculated residual drift ratios for different columns. The calculated residual drift ratios are based on both average and average plus standard deviation residual drift spectra. Based on the average residual drift spectra, the ratio of calculated and measured residual drift ratio for NF-1 and NF-2 is 0.9 and 1.1, respectively. Per average plus standard deviation residual drift spectra, the ratio for NF-1 and NF-2 is 1.4 and 1.6, respectively. The ratio for MN and SETN based on the average plus standard deviation residual drift spectra is 1 and 1.1, respectively, and per average residual drift spectra is 0.7 and 0.8, respectively. For NF-1 and NF-2, the average residual drift spectra reasonably estimate the measured residual drift ratio while the average plus standard deviation spectra overestimate it. Conversely, the average plus standard deviation spectra provide a good estimation of the measured residual drift ratio for MN and SETN and the average spectra underestimate it. For ETN, SVTN, and UCSD columns, both average and average plus standard deviation spectra significantly overestimate the measured residual drift ratio. This is due to the fact that the envelops of residual drift spectra were generated by eliminating the valleys in the residual drift spectra, which leads to an overestimation of the residual drift ratio in columns with low residual drift ratios, especially for higher periods.

9 Conclusions

Residual drift spectra for circular cantilever bridge columns reinforced with Gr. 60 under different displacement ductilities, site conditions, and three ranges of S_1 were generated. The following conclusions were made based on the results of the study discussed herein:

1. For both soil (V_{s30} = 360 m/s (1200 ft/s)) and rock (V_{s30} = 760 m/s (2500 ft/s)) sites and all column periods and cracked stiffness ratios, the residual drift ratio is less than one percent when S_1 is less than 0.6 g.

2. In both soil and rock sites with S_1 of 0.4–0.6 g, the displacement ductility demand remains relatively small. The energy in these records is not sufficiently large to place displacement ductilities exceeding two. As S_1 increases, the displacement ductility demands of four and six are generated for S_1 of 0.6–0.8 g and S_1 > 0.8 g, respectively. Furthermore, the residual drift ratio becomes greater with the increase of one-second spectral acceleration, period, and the ratio of the cracked to the gross moment of inertia of the column.

3. For both soil and rock sites with S_1 of 0.6–0.8 g, the residual drift ratio is below 1% for the average data regardless of the column period and the cracked stiffness ratio when the displacement ductility demand is two. When the average plus standard deviation results are considered, the residual drift ratio is below 1% for all periods up to cracked stiffness ratios of 0.5 and 0.3 for soil and rock sites, respectively. Additionally, for both site conditions based on the average plus standard deviation data, the residual drift ratio exceeds 1% for long-period columns (period of at least 1.4 s) when the cracked stiffness ratio is 0.6 or 0.7.

4. In soil sites with S_1 of 0.6–0.8 g and ductility demand of four, the residual drift ratio for all cracked stiffness ratios exceeds 1% as the column period is higher than 0.4 s.

5. The residual drift ratio of a column with ductility demand of two in the rock site with S_1 > 0.8 g is less than 1% for the average data when the cracked stiffness ratio is less than 0.5. In soil sites, the residual drift ratio for all stiffness ratios exceeds 1% for the average data when the column period is at least 1 s.

6. For both sites with S_1 > 0.8 g and ductility demand of four, the residual drift ratio exceeds 1% for all cracked stiffness ratios as the column period exceeds 0.5 s. For shorter period columns, the residual drift ratio, may exceed 1% depending on the cracked stiffness ratio.

7. When S_1 > 0.8 g and the displacement ductility demand is six, the residual drift ratio exceeds 1% when the column period is at least 0.3 s. This is true regardless of the site conditions considered in this study.

8 A comparison between the residual drift spectra and the experimental data for seven bridge columns indicated that the residual drift spectra can provide a reasonable estimate of high residual drift ratios while it drastically overestimates the low residual drift ratios especially for long-period columns.

Acknowledgement

The study presented in this paper was funded by a grant from the Federal Highway Administration under Contract No. DTFH61-07-C-00031. The support of Dr. Philip Yen, FHWA program director, is appreciated. The opinions expressed in this paper belong solely to the authors and do not necessarily represent the views of the sponsor.

References

Aagaard BT, Brocher TM, Dolenc D, Dreger D, Graves RW, Harmsen S, Hartzell S, Larsen S, McCandless K, Nilsson S, Petersson NA, Rodgers A, Sjögreen B and Zoback ML (2008), "Ground-Motion Modeling of the 1906 San Francisco Earthquake, Part II: Ground-Motion Estimates for the 1906 Earthquake and Scenario Events," *Bulletin of the Seismological Society of America*, **98**(2): 1012–1046.

Abrahamson NA and Somerville PG (1996), "Effects of the Hanging Wall and Footwall on Ground Motions Recorded During the Northridge Earthquake," *Bulletin of Seismological Society of America*, **86**(1B): 93–99.

American Association of State Highway and Transportation Officials (AASHTO) (2017), *LRFD Bridge Design Specifications*, Washington, D.C.

American Association of State Highway and Transportation Officials (AASHTO) (2002), *LRFD Bridge Design Specifications*, Washington, D.C.

Caltrans (2004), *Bridge Design Specifications*, California Department of Transportation, Sacramento, CA.

Caltrans (2006), *Seismic Design Criteria* (*SDC*), Version 1.4, California Department of Transportation, Sacramento, CA.

Caltrans (2013), "*Seismic Design Criteria* (*SDC*)," Version 1.7, California Department of Transportation, Sacramento, CA.

Cheng H, Li H, Wang D, Sun Z, Li G and Jin J (2016), "Research on the Influencing Factors for Residual Displacements of RC Bridge Columns Subjected to Earthquake Loading," *Bulletin of Earthquake Engineering*, **14**(8): 2229–2257.

Choi H, Saiidi MS and Somerville P (2007), "Effects of Near-Fault Ground Motion and Fault-Rupture on the Seismic Response of Reinforced Concrete Bridges," *Report No. CCEER-07-06*, Center for Civil Engineering Earthquake Research, Department of Civil and Environmental Engineering, University of Nevada, Reno, Nevada.

Choi H, Saiidi MS, Somerville P and El-Azazy S (2010), "Experimental Study of Reinforced Concrete Bridge Columns Subjected to Near-Fault Ground Motions," *ACI Structural Journal*, **107**(1): 3–12.

Chioccarelli E and Iervolino I (2010), "Near-Source

Seismic Demand and Pulse-Like Records: A Discussion for L′Aquila Earthquake," *Earthquake Engineering and Structural Dynamics*, **39**(9): 1039–1062.

Graves RW and Pitarka A (2010), "Broadband Ground-Motion Simulation Using a Hybrid Approach", *Bulletin of Seismological Society of America*, **100**(5A): 2095–2123.

Harikrishnan MG and Gupta VK (2020), "Scaling of Residual Displacements in Terms of Elastic and Inelastic Spectral Displacements for Existing SDOF Systems," *Earthquake Engineering and Engineering Vibration*, **19**(1): 71–85. https://doi.org/10.1007/s11803-020-0548-z

Japan Road Association (JRA) (1996), *Design Specifications of Highway Bridges*, Part V: Seismic Design, Tokyo, Japan.

Kawashima K, MacRae GA, Hoshikuma J and Nagaya K (1998), "Residual Displacement Response Spectrum," *J. Struct. Eng.*, **124**(5): 523–530.

Lee WK and Billington SL (2010), "Modeling Residual Displacements of Concrete Bridge Columns under Earthquake Loads Using Fiber Elements," *J. Bridge Eng.*, **15**(3): 240–249.

Liossatou E and Fardis MN (2015), "Residual Displacements of RC Structures as SDOF Systems," *Earthquake Engineering & Structural Dynamics*, **44**(5): 713–734.

Mackie K and Stojadinovic B (2004), "Residual Displacement and Post Earthquake Capacity of Highway Bridges," *13th World Conference on Earthquake Engineering*, Vancouver, B.C., Canada.

McKenna F, Fenves GL and Scott MH (2006), *OpenSees: Open System for Earthquake Engineering Simulation*, Pacific Earthquake Engineering Research Center, University of California Berkeley, CA. http://opensees.berkeley.edu

Phan VT, Saiidi MS and Anderson JG (2005), "Near Fault (Near Field) Ground Motion Effects on Reinforced Concrete Bridge Columns," *Report No. CCEER-05-07*, Center for Civil Engineering Earthquake Research, Department of Civil and Environmental Engineering, University of Nevada, Reno, Nevada.

Phan VT, Saiidi MS, Anderson J and Ghasemi H (2007), "Near-Fault Ground Motion Effects on Reinforced Concrete Bridge Columns," *J. Struct. Eng.*, **133**(7): 982–989.

Ruiz-Garcia J and Miranda E (2005), "Residual Displacement Ratios for Assessment of Existing Structures," *Earthquake Engineering and Structural Dynamics*, **35**(3): 315–336.

Saiidi MS and Seyed Ardakani SM (2012), "An Analytical Study of Residual Displacement in RC Bridge Columns Subjected to Near-Fault Earthquakes," *Bridge Structures*, **8**(1): 35–45.

Seyed Ardakani SM and Saiidi MS (2013), "Design of Reinforced Concrete Bridge Columns for Near-Fault Earthquakes," *Report No. CCEER-13-13*, Center for Civil Engineering Earthquake Research, Department of Civil and Environmental Engineering, University of Nevada, Reno, Nevada.

Seyed Ardakani SM and Saiidi MS (2018), "Simple Method to Estimate Residual Displacement in Concrete Bridge Columns Under Near-Fault Earthquake Motions," *Engineering Structures*, **176**: 208–219.

Somerville PG, Smith NF, Graves RW and Abrahamson NA (1997), "Modification of Empirical Strong Ground Motion Attenuation Relations to Include the Amplitude and Duration Effects of Rupture Directivity," *Seismological Research Letters*, **68**(1): 199–222.

Somerville PG (1998), "Development of an Improved Representation of Near-Fault Ground Motions," *Proc. of the SMIP98 Seminar on Utilization of Strong-Motion Data*, Oakland, CA, 1–20.

Somerville PG (2002), "Characterizing Near Fault Ground Motion for the Design and Evaluation of Bridges," *Proceedings of the Third National Seismic Conference and Workshop on Bridges and Highways*, Portland, OR, 137–148.

Somerville PG, Graves RW, Collins NF, Song SG, Ni S and Cummins P (2009), "Source and Ground Motion Models of Australian Earthquakes," *Proc. of the 2009 Annual Conference of the Australian Earthquake Engineering Society*, Newcastle, Australia, 1–9.

Terzic V, Schoettler MJ, Restrepo JI and Mahin SA (2015), "Concrete Column Blind Prediction Contest 2010: Outcomes and Observations," *PEER Report No. 2015/01*, Pacific Earthquake Engineering Research Center, Headquarters at the University of California, Berkeley.

Wang X, Shafieezadeh A and Ye A (2019), "Optimal EDPs for Post-Earthquake Damage Assessment of Extended Pile-Shaft-Supported Bridges Subjected to Transverse Spreading," *Earthquake Spectra*, **35**(3): 1367–1396.

Yazgan U and Dazio A (2011), "Simulating Maximum and Residual Displacements of RC Structures: I. Accuracy," *Earthquake Spectra*, **27**(4): 1187–1202.